catalysts

MDPI

Article

Modification of High Surface Area Carbons using Self-limited Atomic Layer Deposition

Mengjie Fan, Kai Shen, Raymond J. Gorte, and John M. Vohs*

Department of Chemical and Biomolecular Engineering, University of Pennsylvania, Philadelphia, PA 19104, USA

*Correspondence: vohs@seas.upenn.edu

Abstract: This study explores the application of Atomic Layer Deposition (ALD) for functionalizing high-surface-area carbon supports with metal and metal oxide films and particles for applications in catalysis and electrocatalysis. The work reported here demonstrates that through careful choice of precursors and absorption and reaction conditions, self-limited ALD growth on a high surface area carbon support can be achieved. Specific examples that are presented include the growth of conformal films of ZrO_2 and SnO_2 and the deposition of Ga_2O_3 and Pt particles on a carbon black support with a surface area of 250 $m^2 \cdot g^{-1}$. A novel strategy for controlling the Pt weight loading and producing sub-nanometer Pt particles on a carbon support using a single ALD cycle is also presented.

Keywords: Carbon black; ALD; Metal oxide; Metal;

1. Introduction

Carbon in its various forms, such as carbon black, graphite, carbon nanotubes, and activated carbon, has a range of properties that make it a useful support material for heterogenous catalysts [1]. These include having a high surface area, good thermal properties, and chemical stability. Additionally, its high electrical conductivity and stability in both basic and acidic environments have led to its wide use as an electrode and catalyst support material in electrochemical devices, including batteries [2], supercapacitors [3], fuel cells [4], and sensors [5]. Specific examples of this include the use of Pt supported on carbon as the anode in low-temperature polymer-exchange membrane fuel cells (PEMFC) [6, 7], and IrO_2 supported on carbon nanotubes as the catalyst for the oxygen evolution reaction in water electrolysis cells [8].

All these applications of carbon as a support material require either surface functionalization or the dispersion of required catalytic components on its surface. These are hindered by the inert nature of carbon which interacts only weakly with supported metals and metal oxides. As a result, the catalytic species deposited by traditional methods, such as impregnation, ion exchange, and precipitation, tend to be in the form of particles with relatively low dispersion. This is particularly problematic for many highly catalytic materials, such as Pt, Pd and IrO_2, where high dispersion is required in order for the electrodes to be cost effective [9-13]. Introducing oxygen containing functional groups on the carbon surface via pretreatment with a strong acid, such as HNO_3 and H_2SO_4, which provide nucleation sites for deposited catalytic species is one approach that has been used to enhance dispersion of catalyst when using these traditional synthesis methods [14, 15], but this tends to still produce surfaces with a low density of catalytic sites.

Recently, ALD has also received much attention as a method to deposit catalytic species on carbon surfaces. In a conventional ALD process a carrier gas is used to expose the growth substrate to a gaseous precursor for the material that is to be deposited (typically an organometallic compound) under conditions where only a single monolayer of the

Citation: To be added by editorial staff during production.

Academic Editor: Firstname Lastname

Received: date
Revised: date
Accepted: date
Published: date

precursor adsorbs. Following adsorption of the precursor the sample is exposed to an oxidizing or reducing environment to remove the ligands on the adsorbed metal center. This cycle is then repeated as many times as necessary to achieve the desired surface coverage or film thickness. For example, Pt can be deposited using cycles consisting of exposure to $Pt(acac)_2$ (acac = acetylacetonate) followed by an oxidation or reduction treatment to remove the acac ligands [16, 17]. The adsorption of a single monolayer of the precursor per cycle makes ALD growth self-limiting and the amount of metal or metal oxide deposited is determined by the size and number of ligands on the metal center. ALD has the advantage of providing precise control over the structure of the deposited material and in many cases can produce conformal films of both metals and metal oxides on a range of substrates [18-21].

The formation of conformal films on carbon supports using ALD, however, presents several challenges. First, for high-surface-area carbons, such as those used in catalytic applications, diffusion of the precursor into the nanopores of the carbon can be limiting and, if not accounted for, can result in less than saturation coverage of the adsorbed precursor, causing inhomogeneous growth and low per cycle growth rates. This is especially problematic when the carbon support is exposed to the precursor using a carrier gas at atmospheric pressure [22]. For example, Fiorentino et al. used ALD to deposit Al_2O_3 and TiN on carbon nanotube bundles and found that only 25 % of the surface of the nanotubes were coated which they attributed to diffusion limiting penetration of the ALD precursors deep into the nanotube bundle [23]. Second, the adsorbed precursor molecules typically interact weakly with carbon surfaces. This requires the temperature used during precursor exposure to be chosen carefully to ensure that a saturated monolayer of adsorbed precursor is formed.

While numerous papers can be found in the literature in which ALD has been used to deposit catalytic materials on carbon supports [24, 25], many of these studies show unusually low per cycle deposition rates, indicating that conventional self-limited ALD growth was not achieved. While the materials produced in these studies may still have quite interesting structures and useful catalytic properties, it may be advantageous to obtain true self-limited ALD growth on high-surface-area carbon support materials for some catalytic applications. True, self-limited growth would provide a more efficient means to functionalize the entire carbon surface, control the size of deposited metal particles, and produce ultrathin conformal films whose catalytic properties could be more easily optimized than the bare carbon surface.

The goal of this study was to explore the use of ALD to modify carbon surfaces using conditions where self-limited growth was obtained via reaction of an adsorbed monolayer of the gaseous precursor, as demonstrated via quantitative analysis of the ALD deposition rates. Examples that will be presented include ALD growth of films of SnO_2 and ZrO_2, and the ALD deposition of Ga_2O_3 and Pt particles. A strategy for controlling the Pt particle size using ALD is also presented.

2. Results and Discussion

2.1. ALD of metal oxide films on carbon

Our initial studies focused on the growth of conformal oxide films on the high-surface-area carbon black support. The specific oxide films that were grown were ZrO_2, SnO_2, and Ga_2O_3. Tin oxide and zirconium oxide were chosen because the organometallic precursors, $SnCl_4$ and tetrakis(dimethylamido)zirconium (TDMAZ), can be oxidized at the ALD growth temperature via exposure to H_2O. For Ga_2O_3, $Ga(TMHD)_3$ (TMHD = 2,2,6,6-tetramethyl-3,5-heptanedionate) was used as the precursor; and a high temperature (673 K) air oxidation step was used to remove the ligands and form the oxide. This precursor was chosen because TMHD is a common ligand that is used in many organometallic ALD precursors.

To demonstrate that self-limited growth was obtained, the sample mass as a function of the number ALD cycles was measured for the growth of the ZrO_2, SnO_2, and Ga_2O_3 films and are displayed in Figure 1. Gravimetrically measured deposition rates in units of number of metal atoms deposited per m^2 per ALD cycle for the three oxides are also listed in Table 1. Figure 1 shows that, in all three cases, the growth curves were nearly linear, which is consistent with self-limited growth; however, as shown in Table 1 the amount deposited per cycle varied somewhat between the oxides.

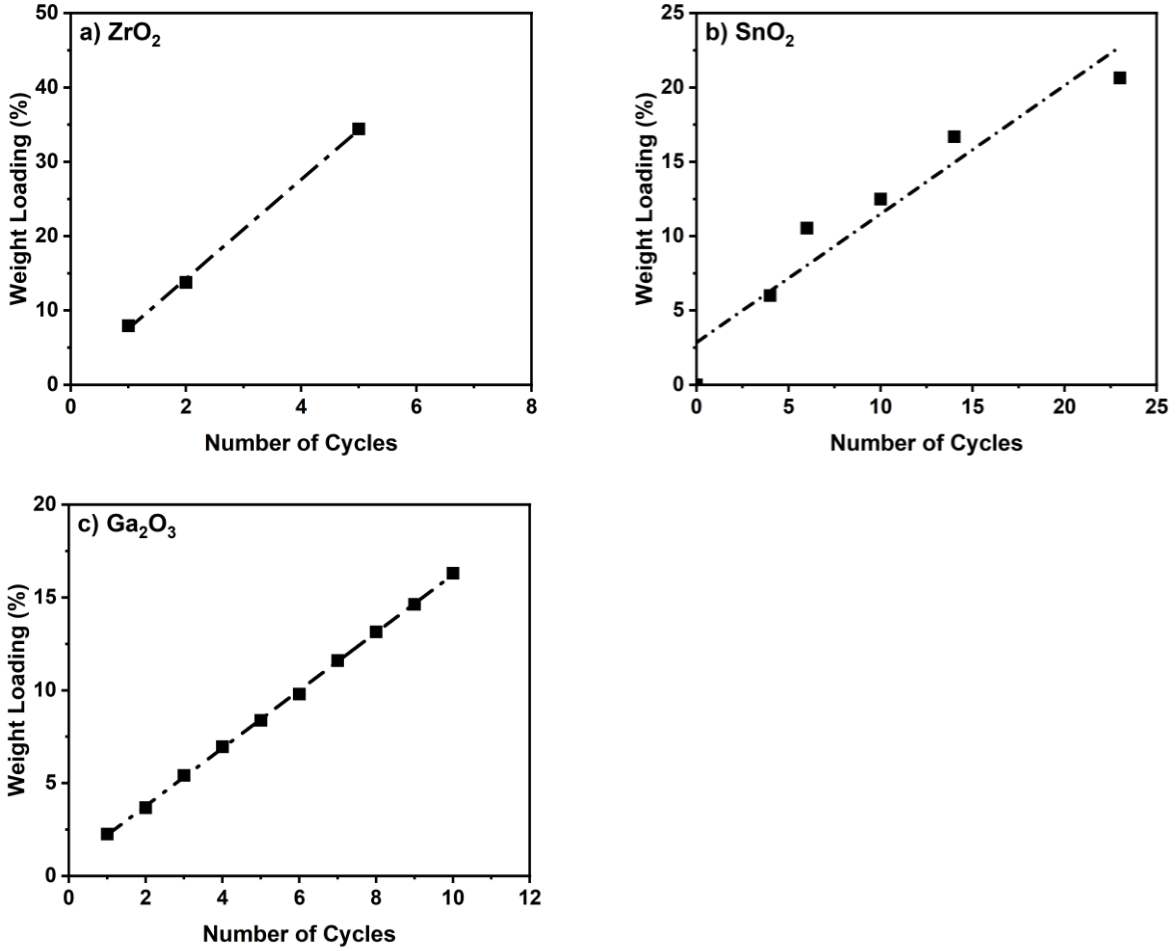

Figure 1. % Weight loading as a function of ALD cycles for a) ZrO_2, b) SnO_2, and c) Ga_2O_3 on carbon black support with an initial surface area of 250 m^2/g.

Table 1. Summary of ALD procedure and growth rate

Component	Ligand	Growth rate on carbon per cycle
ZrO_2	TDMA	1.3×10^{18} atoms/m^2
SnO_2	Chloride	1.0×10^{17} atoms/m^2
Ga_2O_3	TMHD	4.0×10^{17} atoms/m^2
Pt	acac	1.3×10^{18} atoms/m^2

For the ZrO_2 film which was grown using TDMAZ as the precursor with adsorption and oxidation steps at 453 K, a ZrO_2 weight loading of 34 % was achieved after only five ALD cycles, which corresponds to a deposition rate of 1.3×10^{18} Zr atoms·m^{-2}·$cycle^{-1}$ (Table 1). It is useful to compare this deposition rate on carbon with what has been reported previously for the ALD growth of ZrO_2 films using the same precursor on other supports.

While values for the ZrO_2 deposition rates vary somewhat from study-to-study, reported values are typically between 0.1 and 0.2 nm·cycle^{-1} [26-31]. For example, Shim et al. report a growth rate of 0.15 nm·cycle^{-1} on a Si_3N_4-coated planar Si(100) substrate at 523 K using TDMAZ. This corresponds to a metal atom deposition rate of 4.2×10^{18} Zr atoms·m^{-2}·cycle^{-1} which is comparable to that obtained here for growth on carbon black.

It is also useful to estimate how many ALD cycles would be required to grow a monolayer, conformal film of ZrO_2 on the carbon support. The density of Zr atoms on an ideal ZrO_2(100) surface of cubic zirconia is 7.5×10^{18} Zr atoms·m^{-2}. Assuming that a monolayer ZrO_2 film on the carbon support would have a similar Zr atom density, for the measured Zr atom deposition rate, ~6 ALD cycles would be required to completely cover the support. This value seems reasonable when one accounts for the large size of the dimethylamino ligands on the Zr precursor.

As shown in Figure 1b, while a linear growth curve was obtained for SnO_2 deposition at 423 K using water as the oxidant, the increase in mass per ALD cycle was substantially less than that for ZrO_2 deposition. For SnO_2, 23 ALD cycles produced a 21 wt % loading of the oxide. This mass change corresponds to a Sn atom deposition rate of 1.0×10^{17} Sn atoms·m^{-2}·cycle^{-1}. Using the SnO_2(100) surface to estimate the density of Sn atoms in monolayer SnO_2 film gives a value of 4.4×10^{18} Sn atoms·m^{-2}. Together these values indicate that ~40 ALD cycles would be required to coat the surface of the carbon support with a monolayer film of SnO_2.

Unlike that for ZrO_2 ALD, the SnO_2 deposition rate is substantially less than what has been reported in the literature for SnO_2 ALD on other supports. For example, Sundqvist *et al.* [32] report that, when using a SnI_4 precursor to grow SnO_2 on a single crystal α-Al_2O_3(012) surface, the growth rate was ~0.1 nm·cycle^{-1}. This corresponds to a Sn atom deposition rate of 2.8×10^{18} Sn atoms·m^{-2}·cycle^{-1} which is over an order of magnitude higher than what was obtained here for growth on carbon. This difference in the deposition rate on carbon and an oxide surface is likely a result of how Sn halide precursors interact with the two surfaces. On alumina, SnI_4 (which would be expected to have a reactivity similar to the $SnCl_4$ used here) would adsorb dissociatively to form strongly chemisorbed species, resulting in a relatively stable monolayer of the adsorbed precursor. In contrast, SnI_4 (or $SnCl_4$) will likely not dissociate and only exhibit van der Waals interactions with the unreactive carbon surface. This makes it harder to maintain a saturation coverage of the precursor and may result in some of it desorbing intact during the water oxidation step. While the situation may be similar for the TDMAZ precursor used for ZrO_2 growth, the large dimethylamino ligands in this molecule would result in stronger Van der Waals interactions with the surface compared to $SnCl_4$, thereby producing a more stable adsorbed precursor layer.

The TMHD ligands in the $Ga(TMHD)_3$ precursor used for ALD deposition of Ga_2O_3 are significantly less reactive than those in the Sn and Zr precursors used in this study and could not be removed by exposure to H_2O at the growth temperature. Thus, for ALD growth of Ga_2O_3, a different procedure was used. As described in the Materials and Methods section, each ALD cycle for Ga_2O_3 deposition consisted of exposing the evacuated carbon support to $Ga(TMHD)_3$ at 523 K, followed by heating the sample to 673 K and then exposing it to air for 10 min. As shown in Figure 1c this procedure also produced a linear growth curve with a 16 wt % loading of Ga_2O_3 obtained after 10 ALD cycles. This corresponds to a Ga deposition rate of 4.0×10^{17} Ga atoms·m^{-2}·cycle^{-1}. This deposition rate is essentially the same as that reported by Ramachandran et al. for ALD growth of Ga_2O_3 on an oxidized Si wafer using $Ga(TMHD)_3$ [33]. It is again useful to use the measured Ga atom deposition rate to estimate how many ALD cycles would be required to form a complete monolayer Ga_2O_3 film on the carbon support. Using the density of Ga atoms on the β-Ga_2O_3(100) surface (5.6×10^{18} Ga atoms·m^{-2}) to define a monolayer, we estimate that ~14 ALD Ga cycles would be required.

STEM, TEM and EDS elemental scans were used to characterize the structure of the deposited oxide films on the carbon black support. Figure 2 displays these images for a 5

ALD cycle ZrO_2/C sample. The large TEM image in this figure shows that the carbon black support is composed of carbon particles that are 30-80 nm in diameter. The right side of the figure shows C, O, and Zr EDS elemental scans that were obtained from the designated region in the smaller STEM image. The EDS data show a strong correlation between C, O, and Zr elemental scans. This demonstrates that the ZrO_2 film covers nearly all the surface of the carbon support. The conformal nature of the ZrO_2 film is further confirmed by the slightly higher intensity in the O and Zr signals around the edges of the carbon particles. In these positions the electron beam is passing through a cross-section of the film which produces a higher signal than when the beam is more perpendicular to the film which is the case when it is positioned in the middle of one of the carbon particles. It is also noteworthy that 5 ZrO_2 ALD cycles were sufficient to completely cover the carbon surface, consistent with the analysis of the growth rate data presented above which indicated that ~6 cycles would be required to completely coat the surface.

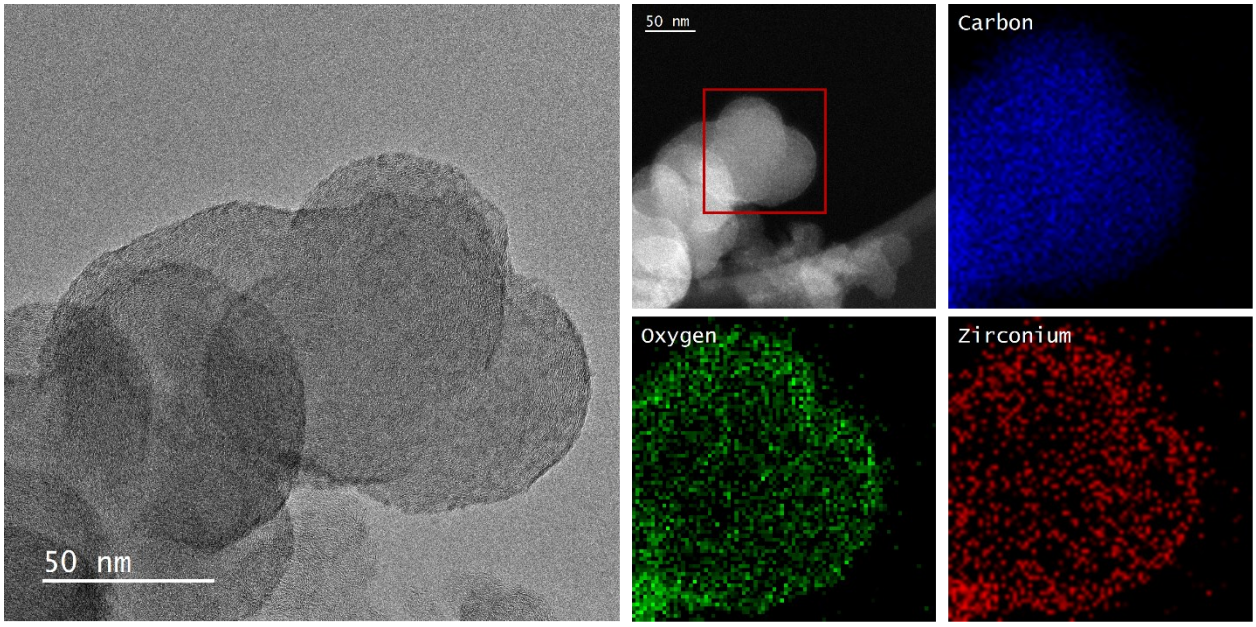

Figure 2. TEM (large image), STEM and EDS images of 5 ALD cycle ZrO_2 on carbon black support after 453 K oxidation with water vapor. The area of the elemental EDS images correspond to the red box in the STEM image.

To evaluate the thermal stability of the ALD-generated ZrO_2 thin film on carbon, the same 5 ALD cycle ZrO_2/C sample was treated in air at 623 K for 10 minutes, followed by structural characterization using TEM. As shown in Figure 3, distinct dark spots are visible in the TEM image, indicating that the heat treatment at 623 K promoted partial agglomeration of the film into particles that are ~2 nm in diameter. The EDS mapping on the right shows the distribution of C, O, and Zr signals. While some particle agglomeration is evident in the TEM image, the overall Zr signal remains well-aligned with C and O, suggesting that the majority of the ZrO_2 remains uniformly distributed on the carbon black surface, with only a small portion aggregating into particles. For applications in electrodes for electrochemical devices, carbon is not likely to be exposed to such high-temperature conditions. Therefore, the mild particle agglomeration observed here after heating to 623 K would not pose a significant issue for these applications.

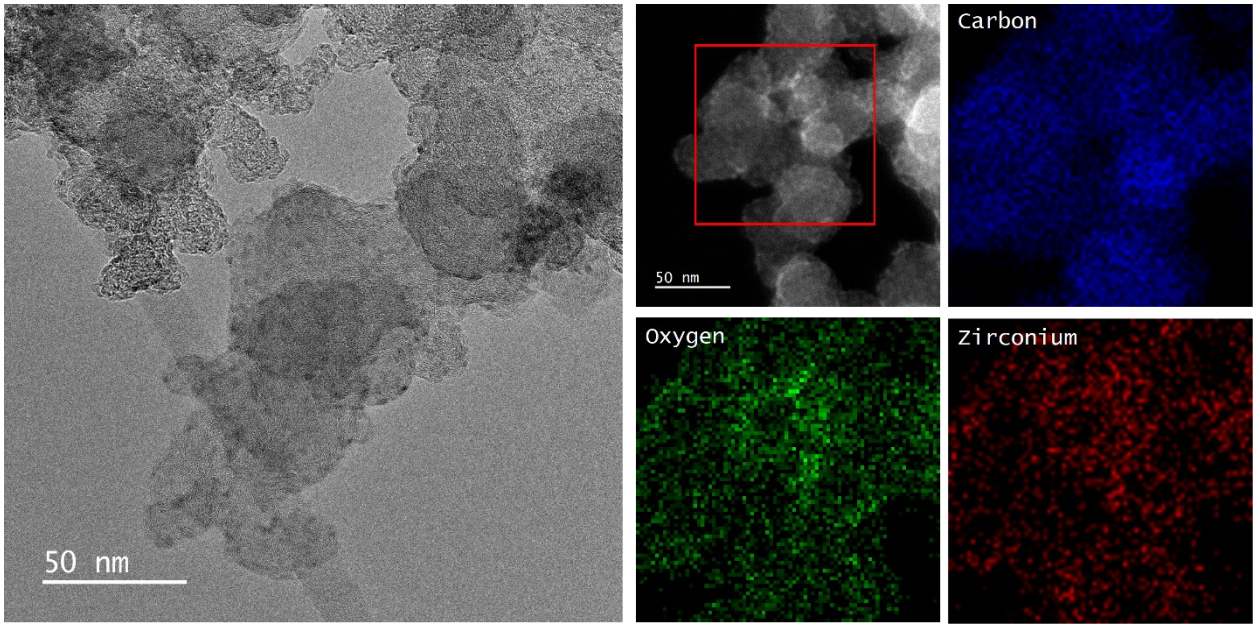

198

Figure 3. TEM (large image), STEM and EDS images of 5 ALD cycle ZrO_2 on carbon black support after 623 K oxidation in air. The area of the elemental EDS images correspond to the red box in the STEM image. 199 200 201

202

A similar set of TEM/EDS images for a 23 ALD cycle SnO_2/C sample is presented in Figure 4. The Sn and O elemental EDS scans obtained from this sample show a film like structure for the SnO_2, but the Sn EDS signal intensity is not uniform over the carbon surface indicating that some islanding has occurred. From the growth rate analysis presented above, it is estimated that ~40 ALD cycles would be required to form a SnO_2 film that completely covers the surface of the support. Based on this estimate, the SnO_2 film in the 23 ALD cycle SnO_2/C sample should cover approximately half of the surface which seems reasonably consistent with the TEM/EDS results. 203 204 205 206 207 208 209 210

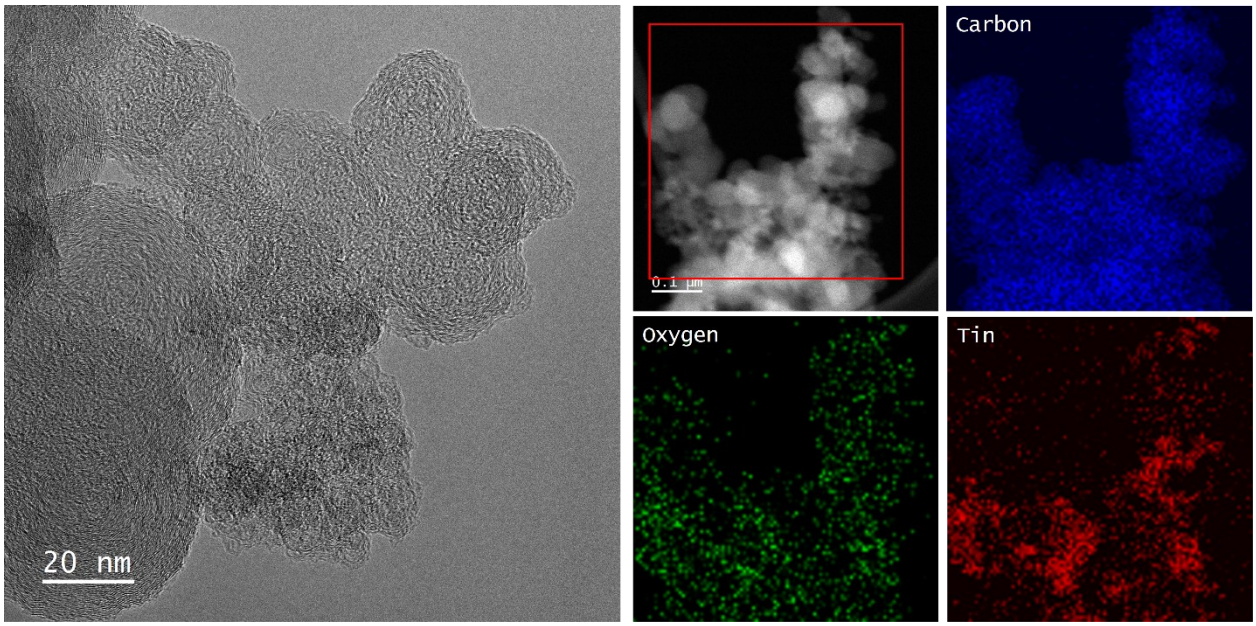

211

Figure 4. TEM (large image), STEM and EDS images of 23 ALD cycle SnO_2 on carbon black support after 423 K oxidation with water. The area of the elemental EDS images correspond to the red box in the STEM image.

For the 23 ALD cycle SnO_2/C sample we also investigated the thermal stability of the SnO_2 film by heating to 623 K (*i.e.* 200 K higher than the growth temperature) for 10 min. TEM/EDS scans obtained from this sample are presented in Figure 5. Similar to the case of ZrO_2, the TEM image contains features that suggest some particle formation may have occurred, but this is not readily evident in the EDS scans suggesting that much of the film nature of the SnO_2 has been maintained. This result, therefore, demonstrates that the ALD deposited SnO_2 has high thermal stability and mostly maintains its film-like structure at elevated temperatures.

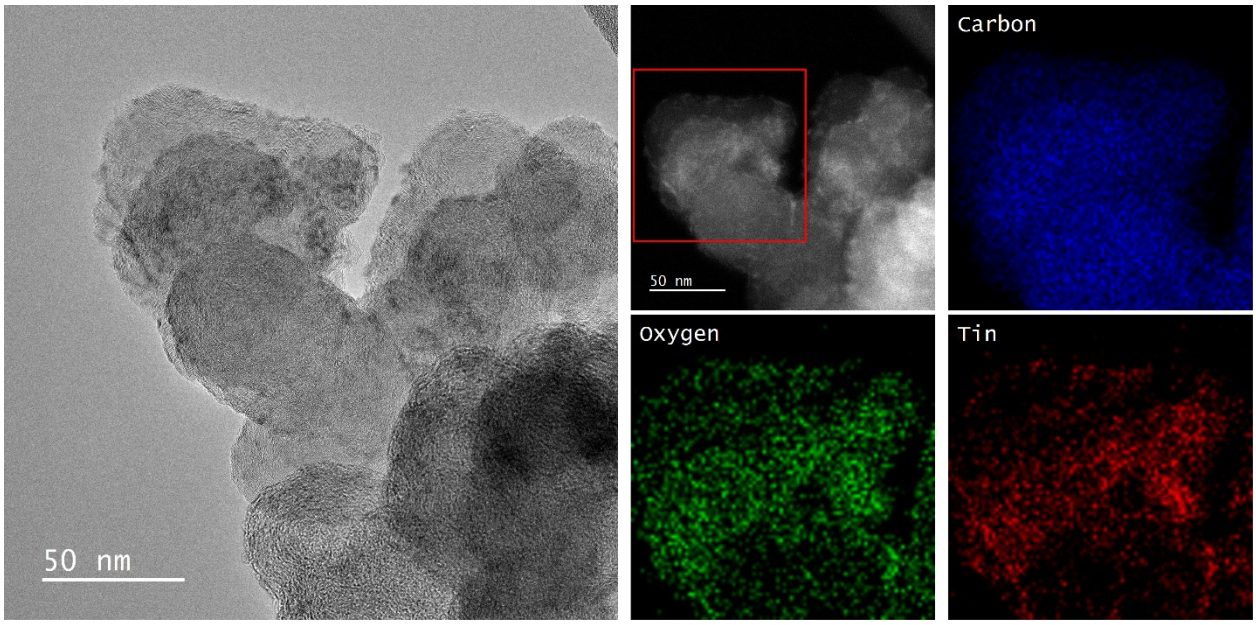

Figure 5. TEM (large image), STEM and EDS images of 23 ALD cycle SnO_2 on carbon black support after 623 K oxidation in air. The area of the elemental EDS images correspond to the red box in the STEM image.

TEM/EDS images for a 10 ALD cycle Ga_2O_3/C sample are displayed in Figure 6. Based on the growth rate analysis presented above, the surface of this sample should be mostly coated with a Ga_2O_3 film. However, in contrast to the ZrO_2 and SnO_2 samples, the TEM and EDS images for this sample clearly show that particle formation has occurred and that the deposited Ga_2O_3 is in the form of 6-7 nm nanoparticles that are distributed evenly across the surface of the carbon black, leaving large regions of the carbon surface uncovered. This difference is likely related to the different conditions that were required to remove the ligands and oxidize the metal center for the different precursors. For the Zr and Sn precursors, this was accomplished by exposing the sample to water vapor at the growth temperature (423 K or 453 K). In contrast for Ga_2O_3 growth the $Ga(TMHD)_3$ precursor was adsorbed at 523 K and then oxidized in air at 673 K. Since the growth rate data indicates that a saturation monolayer coverage of the Ga precursor was obtained during each ALD cycle, it appears that agglomeration and particle formation must have occurred either while heating to 673 K or during oxidation at this temperature.

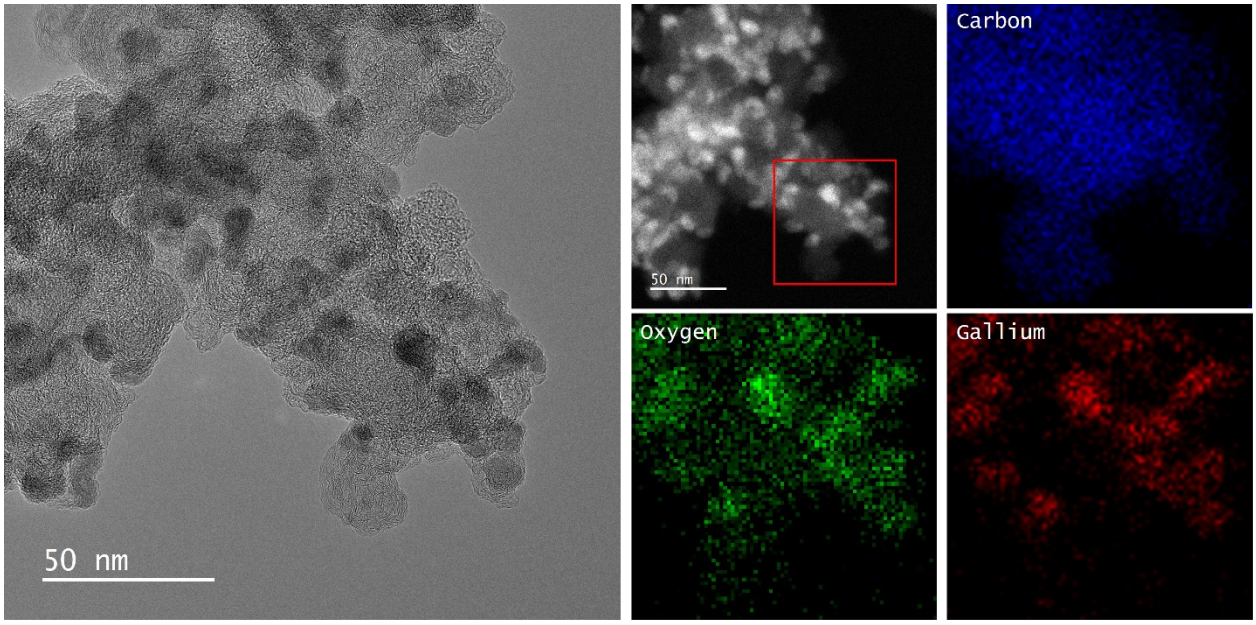

Figure 6. TEM (large image), STEM and EDS images of a 10 ALD cycle Ga_2O_3 on carbon black support after 673 K oxidation. The area of the elemental EDS images correspond to the red box in the STEM image.

2.2. ALD of Pt on carbon

In addition to using ALD for depositing metal oxides on carbon black, we explored the use of ALD to deposit catalytic metals such as Pt. Since the most common way to deposit metals on high surface area supports for catalytic applications is via wet infiltration of an aqueous metal salt solution, followed by drying and reduction, we synthesized a 10 wt % Pt/C sample using this method to provide a base case for comparison to samples synthesized using ALD. STEM and EDS images of this infiltrated sample are displayed in Figure 7a. A histogram showing the particle size distribution obtained from the STEM image is also included in the figure. These data show that the sample produced by infiltration resulted in a bimodal particle-size distribution, with the majority of the particles between 2 and 7 nm in diameter, and a few larger particles between 9 and 10 nm in diameter. It is important to note that, while there are more of the smaller particles, the majority of the Pt is contained in the larger particles. An XRD pattern for this sample, displayed in Figure 8, contains broad peaks at 18° and 25° 2θ due to the carbon black substrate and narrower peaks at 39.7°, 46.2°, and 68° 2θ due to diffraction from the [111], [200], and [220] planes of Pt, respectively. Using the Scherrer equation and the full width at half maximum (FWHM) of the Pt peaks, the Pt particle size in this sample is estimated to be 11 nm, which again demonstrates that the majority of the Pt is in the larger particles.

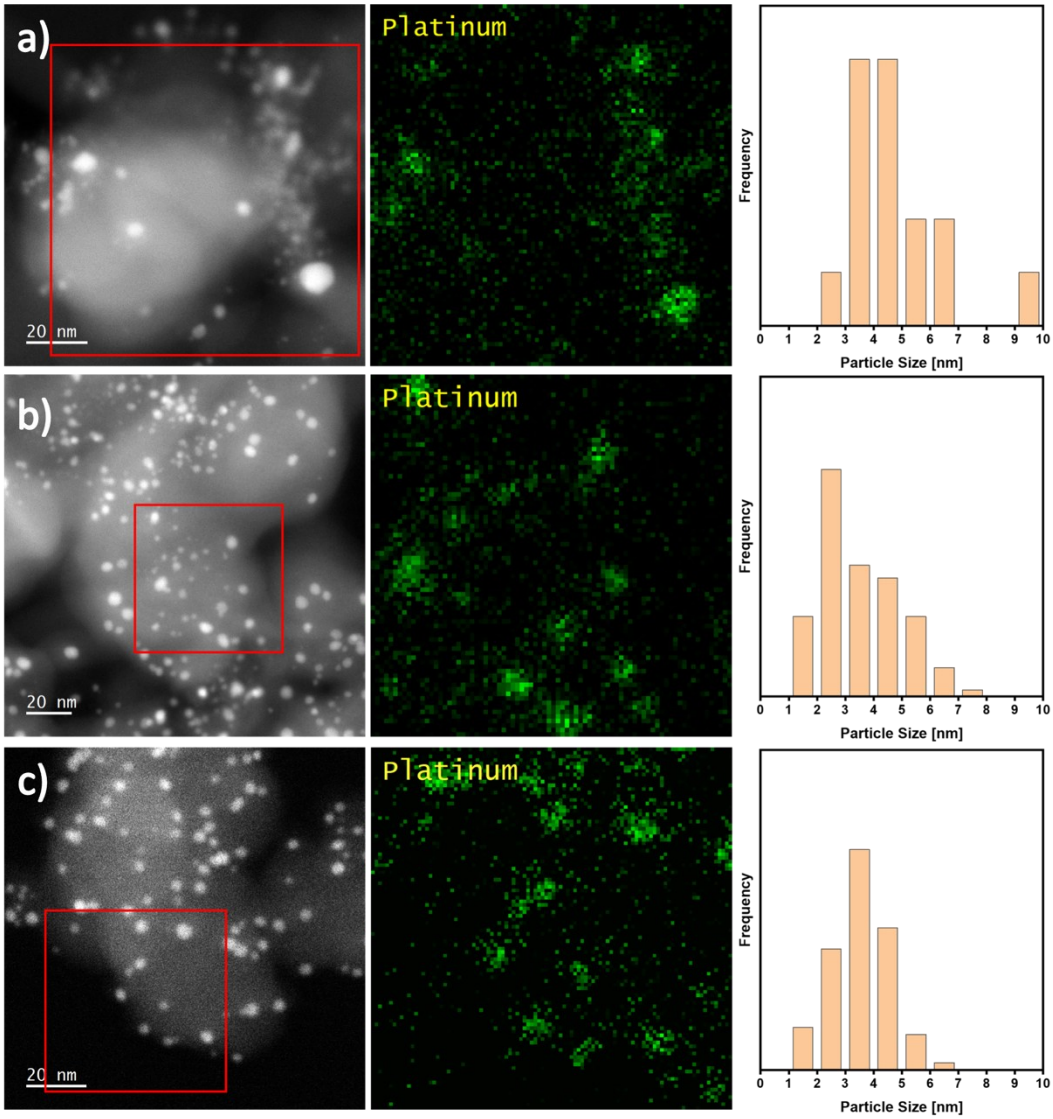

Figure 7. STEM and EDS mapping of a) impregnated 10 wt% Pt on carbon black support after 623 K He-H_2 reduction (average particle size 4.6 nm); b) 1 ALD cycle of Pt on carbon black support (10.4 wt%) after 623 K He-H_2 reduction (average particle size 2.8 nm), and c) 1 ALD cycle of Pt on carbon black support (10.4 wt%) after 773 K He-H_2 reduction (average particle size 3.5 nm). The area of the Pt EDS images correspond to the red box in the STEM images.

Figure 7b displays STEM and EDS images and a particle size histogram for Pt/C sample prepared using a single Pt ALD cycle. Since Pt is an excellent oxidation catalyst, for the $Pt(acac)_2$ precursor the ligands cannot be removed by oxidation, because this also results in combustion of the carbon support. It was found, however, that the acac ligands could be removed by heating in H_2 at 623 K. The Pt weight loading for this sample was 10.4 wt% which corresponds to a Pt deposition rate of 1.3×10^{18} Pt atoms·m^{-2}·$cycle^{-1}$, similar to the Zr deposition rate during ZrO_2 ALD growth and consistent with the adsorption and reaction of a saturated monolayer of the $Pt(acac)_2$ precursor.

The STEM image shows that, even though a monolayer of the precursor was formed during the ALD adsorption step, Pt particle formation occurs during the reduction step. This is not surprising since Pt atoms would be expected to have high mobility on the C

surface at the reduction temperature of 623 K. While both the infiltrated and 1 ALD cycle samples contain ~10 wt % Pt and were reduced in H_2 at 623 K, the particle size distributions for the two samples differ significantly. The histogram shows that a unimodal particle distribution was obtained for the ALD Pt/C sample, with a 2.8-nm, average particle size. The XRD pattern in Figure 8 shows that the Pt diffraction peaks for this sample are also quite broad, with the Scherrer equation giving an average particle size of 3.6 nm. Note that this value is biased toward the larger particles since these contain a larger fraction of the Pt. These results demonstrate that, with carefully chosen conditions, a single Pt ALD cycle can be used to produce a high coverage of 2-3 nm Pt nanoparticles on a carbon support.

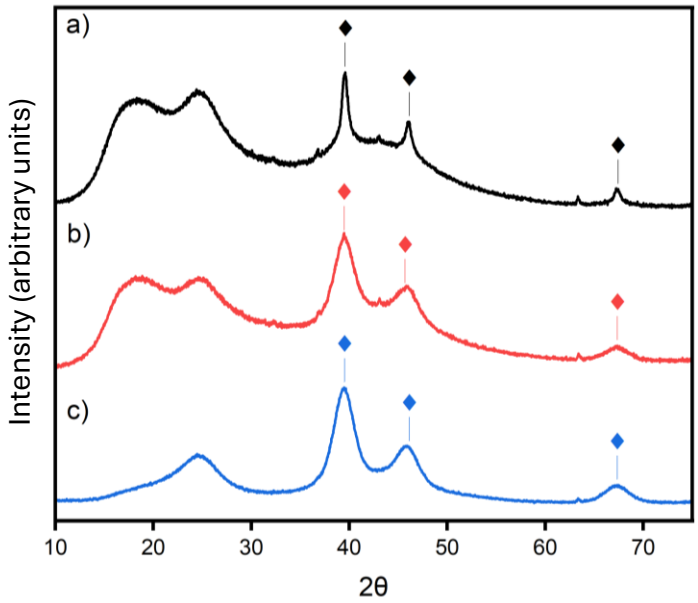

Figure 8. XRD of a) impregnated 10 wt% Pt on carbon black support after 623 K He-H_2 reduction (average particle size 11 nm), b) 1 ALD cycle of Pt on carbon black support after 623 K He-H_2 reduction (average particle size 3.6 nm), and c) 1 ALD cycle of Pt on carbon black support after 773 K He-H_2 reduction (average particle size 3.7 nm). The diamonds designate the peaks that are characteristic of Pt. All of the patterns have the same vertical scale.

The thermal stability of the Pt particles in the ALD Pt/C sample was also investigated by heating the reduced ALD Pt/C sample in H_2 to 773 K for 60 min. A STEM image, EDS map, and particle histogram obtained after this treatment are displayed in Figure 7c. The XRD pattern for this sample is also displayed in Figure 8. These data show that the additional heat treatment resulted in a narrowing of the particle size distribution and an increase in the average particle size from 2.8 nm to 3.5 nm as determined from the histogram data (XRD gives a value of 3.7 nm for this sample). A close examination of the STEM images shows that the primary change upon heating to 773 K was the coalescence of the smallest Pt nanoparticles into the larger 3-4 nm particles, consistent with an Ostwald ripening type process. Even taking into account this sintering, it is noteworthy that ALD Pt deposition followed by heating to high temperature produces a carbon sample with a high coverage of relatively uniform 3-4 nm Pt particles.

To explore the possibility that ALD could be used to produce even smaller Pt particles on the carbon support we modified the ALD procedure by diluting the $Pt(acac)_2$ precursor with liquid acetylacetone (Hacac) and exposing the carbon support to the vapor from this mixture during the ALD adsorption step. The idea here is that the Hacac will compete for adsorption sites with $Pt(acac)_2$. Due to the similarity of the acac ligands and the Hacac, they will both be removed by the 623 K H_2 reduction treatment. The $Pt(acac)_2$ and Hacac will have different adsorption energies on the surface, but the relative coverage

of each in the adsorbed monolayer may be controllable by varying their ratio in the precursor solution. Using this approach, Pt/C samples were prepared using precursor solutions with $Pt(acac)_2$:Hacac ratios of 0.01 and 0.001, resulting in samples with 2-wt% Pt and 0.2-wt% Pt, respectively. STEM images for these samples are presented in Figure 9 and show that the approach was successful in producing smaller Pt particles with a relatively uniform size distribution.

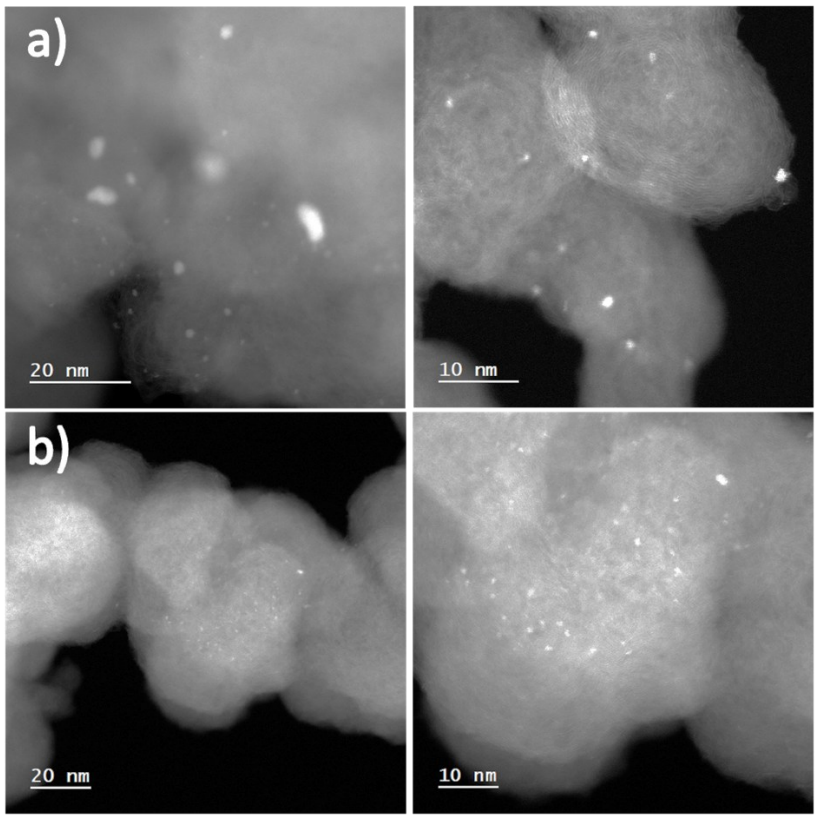

Figure 9. STEM image of 1 ALD cycle of Pt on carbon black support with Hacac dilution targeting a) 2 wt% Pt loading (estimated particle size 1.3 nm), b) 0.2 wt% Pt loading. Both samples were reduced in continuous flow of He-H_2 at 623 K for 1 hr (estimated particle size 0.8 nm). The bright features in each image correspond to Pt particles.

The image of the Pt/C sample prepared using 1 Pt ALD cycle with a precursor solution containing a $Pt(acac)_2$:Hacac ratio of 0.01 in Figure 9a shows that, after reduction in H_2 at 623 K, the carbon support is sparsely covered with Pt particles that are 1 to 2 nm in diameter, significantly smaller than those obtained using pure $Pt(acac)_2$ as the precursor. Decreasing the $Pt(acac)_2$:Hacac ratio to 0.001 produced a sample covered with Pt particles < 1 nm in diameter, as shown in Figure 9b. Since these particles are stable from sintering at temperatures up to 623 K (i.e. the reduction temperature), this synthesis approach provides a relatively easy method to produce very highly dispersed Pt particles on a high surface area carbon support for use in a range of catalytic applications, including those in electrochemistry.

Since alloying with a second metal is often used to alter both the stability and catalytic properties of noble metal catalysts, we also explored the use of ALD to synthesize PtSn alloy particles on the carbon black support. In this work we used 1 Pt ALD cycle to deposit Pt on a carbon black support that had previously been coated with a SnO_2 film using ALD. This SnO_2/C sample had a 21 wt% loading of SnO_2 and had the same structure as that shown in Figure 4. As before, the final step of the Pt ALD step was reduction in H_2 at 623 K for 1 h. In this case, 1 ALD cycle using $Pt(acac)_2$ led to a weight loading of 4.4 wt%. The decreased growth rate compared to Pt/C sample highlights the presence of SnO_2 film and its impact on the adsorption mechanism of $Pt(acac)_2$. STEM and EDS images of

this sample are displayed in Figure 10. The STEM image shows that the carbon support is covered by metal particles with an average diameter of 2.8 nm. The EDS images reveal that Sn did not remain in the form of a conformal film of SnO_2 on the carbon support but had become reduced during the 623 K H_2 reduction step and then migrated to the Pt resulting in the formation of PtSn alloy particles as evidence by the correspondence between the Pt and Sn signals. The XRD pattern for this sample also showed broadening of the Pt diffraction peaks and the appearance of new peaks at 30° and 43° two theta which are characteristic of a PtSn alloy. While we did not further investigate using ALD to produce PtSn alloy particles, but the Pt:Sn ratio in the particles could easily be controlled by varying the amount of SnO_2 deposited on the support prior to Pt ALD.

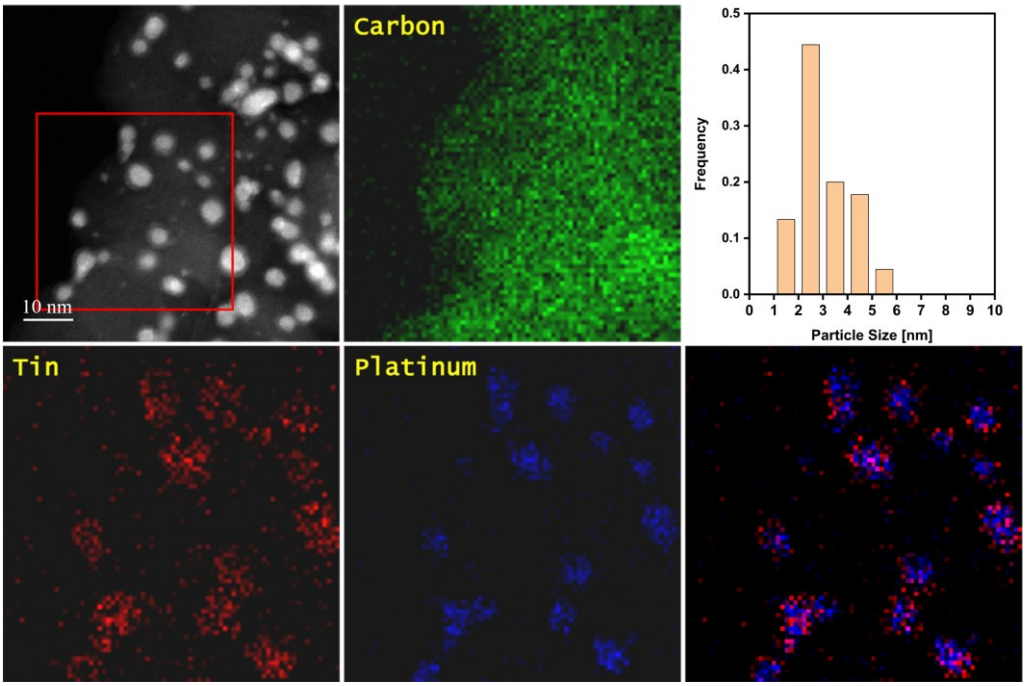

Figure 10. STEM and EDS images of Pt-SnO_2 on carbon black support after reducing in continuous flow of He-H_2 at 623 K for 1 hr. The area of the elemental EDS images correspond to the red box in the STEM image.

3. Materials and Methods

Carbon black (Vulcan XC-72R) with a surface area of 250 m^{-2}·g was used as the support material in this study. To remove any adsorbed species, prior to metal or metal oxide deposition the carbon was pre-treated by heating to 773 K. ALD deposition of Pt, Ga_2O_3, SnO_2, and ZrO_2 onto the carbon support was done using a purpose-built adsorption apparatus that has been described in detail previously [34, 35]. A key feature of this system was that it allowed the sample to be evacuated prior to exposure to the precursor vapor and did not use a carrier gas, features that are needed to limit pore diffusional limitations and achieve conformal growth on high surface area materials [22]. A typical ALD cycle consisted of (1) evacuating the substrate and heating it to the desired deposition temperature, (2) exposing the evacuated substrate to the precursor vapor, (3) evacuation to remove excess precursor vapor, and (4) an oxidation or reduction treatment to remove the ligands on the adsorbed precursor. Films of SnO_2 and ZrO_2 were grown with the carbon support material held at 423 K using $SnCl_4$ (98%, Sigma-Aldrich) and at 473 K using $[(CH_3)_2N]_4Zr$ (tetrakis(dimethylamino)zirconium, TDMAZ, 99%, Strem) as the precursors. These temperatures were chosen because they were found to be low enough to prevent

chemical vapor deposition and high enough to allow for adsorption of a precursor monolayer and not the formation of adsorbed multilayers. The chloride and dimethylamino ligands could be removed and the metal center oxidized by exposure to water vapor with the sample held at the growth temperature. For Ga_2O_3 deposition, $Ga(TMHD)_3$ (TMHD = 2,2,6,6-tetramethyl-3,5-heptanedionate, 99%, Strem) was used as the precursor and the substrate was held at 523 K during the exposure. This higher adsorption temperature was required here to prevent formation of multilayers of the adsorbed $Ga(TMHD)_3$. The TMHD ligand was removed by oxidizing in air at 673 K for 10 min at the end of each deposition cycle.

Deposition of Pt on carbon black was achieved using $Pt(acac)_2$ (acac = acetylacetonate, 98%, Strem) as the precursor at 443 K and the ligands were removed by reduction in flowing 5% H_2-He at 623 K for 1 hr. In some cases, the $Pt(acac)_2$ precursor was mixed with Hacac (Acetylacetone, 99%, Sigma-Aldrich) and the vapor form of the mixture was exposed to the carbon support during ALD growth. To provide a base case Pt/C sample for comparison, a Pt/C sample containing 10 wt % Pt was also prepared using conventional wet impregnation. The impregnation solution was prepared by dissolving the required amount of tetraammineplatinum(II) nitrate ($Pt(NH_3)_4(NO_3)_2$, 99.99%, Alfa Aesar) in a solution containing 75 vol % water and 25 vol % ethanol. The carbon support powder was then added to the solution and the mixture was stirred for several minutes. This mixture was then left in an oven at 343 K overnight to evaporate the solvents. The dried powder was then reduced in a flowing stream of 5% H_2 in He at 623 K for 1 h.

The surface area of the carbon black substrate was determined using BET analysis of N_2 adsorption isotherm at 77 K that was measured using a home-built adsorption apparatus. A Rigaku MiniFlex diffractometer with a Cu-Kα source was used to perform X-ray Diffraction (XRD). A JEOL NEOARM was used to collect transmission electron microscopy (TEM) and energy dispersive X-ray spectra (EDS) images, and a JEOL F200 was used to collect transmission electron microscopy (TEM) images. Sample preparation for STEM/TEM analysis consisted of suspending the sample in ethanol and sonicating to achieve high dispersion. The solution was then added dropwise onto a carbon-coated copper TEM grid (Electron Microscopy Sciences, USA).

4. Summary

In this study we have demonstrated that through careful choice of adsorption and reaction conditions, and by using a vacuum ALD apparatus that helps reduce diffusional limitations, self-limiting ALD growth of a range of materials on high surface area carbon supports can be obtained. Our findings further demonstrate that ALD can provide a high degree of control over both the amount and the structure of the catalytic components that are deposited.

Quantitative analysis demonstrated that for most of the films grown in this study the number of metal atoms deposited per ALD cycle was consistent with the adsorption and subsequent reaction of an adsorbed monolayer of the precursor. For the ALD deposition of ZrO_2 and SnO_2 using TDMAZ and $SnCl_4$ precursors, respectively, the growth of conformal films on the carbon support was achieved. These films exhibited good thermal stability undergoing only modest agglomeration upon heating to 623 K. In contrast, during ALD growth of Ga_2O_3 the higher oxidation temperature, 673 K, required to remove the ligands on the $Ga(TMHD)_3$ precursor resulted in the formation of Ga_2O_3 particles.

For Pt ALD it was found that reduction in H_2 was required to remove the ligands on the $Pt(acac)_2$ precursor. Due to Pt's high catalytic activity using an oxidation treatment for this purpose results in combustion of the carbon support. A single Pt ALD cycle followed by heating to 773 K in H_2 was found to produce a surface covered with a high concentration of Pt particles and a relatively narrow particle size distribution with an average size of 3.5 nm. Furthermore, it was shown that both the amount of Pt deposited, and the average Pt particle size could be controlled during ALD deposition by diluting the $Pt(acac)_2$ in Hacac and using the vapor from this mixture as the ALD precursor. Using this method, it

was demonstrated that Pt particles with an average size less than 1 nm in diameter could be synthesized on a high surface area carbon support using a single ALD cycle. Finally, it was demonstrated that by depositing Pt on top of a preformed SnO_2 film followed by reduction in H_2 produced PtSn alloy particles on the carbon support.

Author Contributions: Conceptualization M.F., R.J.G., J.M.V.; Investigation M.F., K.S.; Project Administration R.J.G., J.M.V.; Writing - original draft M.F.; Writing - review & editing M.F., R.J.G., J.M.V.

Funding: This work was supported by the National Science Foundation grant no. DMREF-2323701 Some of the work was performed at the Singh Center for Nanotechnology at the University of Pennsylvania, a member of the National Nanotechnology Coordinated Infrastructure (NNCI) network, which is supported by the National Science Foundation (GrantNNCI-2025608).

Data Availability Statement: All data is contained in the article.

Conflicts of Interest: The authors declare no conflicts of interest.

References

1. Flandrois, S., and B. Simon. "Carbon Materials for Lithium-Ion Rechargeable Batteries." *Carbon* 37, no. 2 (1999): 165-80.
2. Yuan, Shuang, Qinghao Lai, Xiao Duan, and Qiang Wang. "Carbon-Based Materials as Anode Materials for Lithium-Ion Batteries and Lithium-Ion Capacitors: A Review." *Journal of Energy Storage* 61 (2023): 106716.
3. Lobato-Peralta, Diego Ramón, Patrick U. Okoye, and Cinthia Alegre. "A Review on Carbon Materials for Electrochemical Energy Storage Applications: State of the Art, Implementation, and Synergy with Metallic Compounds for Supercapacitor and Battery Electrodes." *Journal of Power Sources* 617 (2024): 235140.
4. Jaleh, Babak, Mahmoud Nasrollahzadeh, Mahtab Eslamipanah, Atefeh Nasri, Ensiye Shabanlou, Nilesh R. Manwar, Radek Zboril, Paolo Fornasiero, and Manoj B. Gawande. "The Role of Carbon-Based Materials for Fuel Cells Performance." *Carbon* 198 (2022): 301-52.
5. Gibi, Chinchu, Cheng-Hua Liu, Scott C. Barton, Sambandam Anandan, and Jerry J. Wu. "Carbon Materials for Electrochemical Sensing Application – a Mini Review." *Journal of the Taiwan Institute of Chemical Engineers* 154 (2024): 105071.
6. Antolini, Ermete. "Carbon Supports for Low-Temperature Fuel Cell Catalysts." *Applied Catalysis B: Environmental* 88, no. 1 (2009): 1-24.
7. Trogadas, Panagiotis, Thomas F. Fuller, and Peter Strasser. "Carbon as Catalyst and Support for Electrochemical Energy Conversion." *Carbon* 75 (2014): 5-42.
8. Badam, Rajashekar, Masanori Hara, Hsin-Hui Huang, and Masamichi Yoshimura. "Synthesis and Electrochemical Analysis of Novel Iro2 Nanoparticle Catalysts Supported on Carbon Nanotube for Oxygen Evolution Reaction." *International Journal of Hydrogen Energy* 43, no. 39 (2018): 18095-104.
9. Olowoyo, J. O., V. S. Gharahshiran, Y. Zeng, Y. Zhao, and Y. Zheng. "Atomic/Molecular Layer Deposition Strategies for Enhanced Co(2) Capture, Utilisation and Storage Materials." *Chem Soc Rev* 53, no. 11 (2024): 5428-88.
10. Kinoshita, K. "Particle Size Effects for Oxygen Reduction on Highly Dispersed Platinum in Acid Electrolytes." *Journal of The Electrochemical Society* 137, no. 3 (1990): 845.
11. Mukerjee, Sanjeev, and James McBreen. "Effect of Particle Size on the Electrocatalysis by Carbon-Supported Pt Electrocatalysts: An in Situ Xas Investigation." *Journal of Electroanalytical Chemistry* 448, no. 2 (1998): 163-71.
12. Zhou, Weijiang, Miao Li, Ovi Lian Ding, Siew Hwa Chan, Lan Zhang, and Yanhong Xue. "Pd Particle Size Effects on Oxygen Electrochemical Reduction." *International Journal of Hydrogen Energy* 39, no. 12 (2014): 6433-42.
13. Abbott, Daniel F, Dmitry Lebedev, Kay Waltar, Mauro Povia, Maarten Nachtegaal, Emiliana Fabbri, Christophe Copéret, and Thomas J Schmidt. "Iridium Oxide for the Oxygen Evolution Reaction: Correlation between Particle Size, Morphology, and the Surface Hydroxo Layer from Operando Xas." *Chemistry of Materials* 28, no. 18 (2016): 6591-604.
14. Gopiraman, Mayakrishnan, Sundaram Ganesh Babu, Zeeshan Khatri, Wei Kai, Yoong Ahm Kim, Morinobu Endo, Ramasamy Karvembu, and Ick Soo Kim. "An Efficient, Reusable Copper-Oxide/Carbon-Nanotube Catalyst for N-Arylation of Imidazole." *Carbon* 62 (2013): 135-48.
15. Shen, Jianfeng, Weishi Huang, Liping Wu, Yizhe Hu, and Mingxin Ye. "Study on Amino-Functionalized Multiwalled Carbon Nanotubes." *Materials Science and Engineering: A* 464, no. 1 (2007): 151-56.
16. Shen, Kai, Siwon Lee, Ohhun Kwon, Mengjie Fan, Raymond J. Gorte, and John M. Vohs. "Effect of Perovskite-Fluorite Phase Transition on the Catalytic Activity of Pt/Cefeox." *ACS Catalysis* 13, no. 16 (2023): 11144-52.
17. Mao, Xinyu, Alexandre C. Foucher, Tiziano Montini, Eric A. Stach, Paolo Fornasiero, and Raymond J. Gorte. "Epitaxial and Strong Support Interactions between Pt and Lafeo3 Films Stabilize Pt Dispersion." *Journal of the American Chemical Society* 142, no. 23 (2020): 10373-82.
18. Leskelä, Markku, and Mikko Ritala. "Atomic Layer Deposition (Ald): From Precursors to Thin Film Structures." *Thin Solid Films* 409, no. 1 (2002): 138-46.

19. Knisley, Thomas J., Lakmal C. Kalutarage, and Charles H. Winter. "Precursors and Chemistry for the Atomic Layer Deposition of Metallic First Row Transition Metal Films." *Coordination Chemistry Reviews* 257, no. 23 (2013): 3222-31.
20. Johnson, Richard W., Adam Hultqvist, and Stacey F. Bent. "A Brief Review of Atomic Layer Deposition: From Fundamentals to Applications." *Materials Today* 17, no. 5 (2014): 236-46.
21. Ponraj, Joice Sophia, Giovanni Attolini, and Matteo Bosi. "Review on Atomic Layer Deposition and Applications of Oxide Thin Films." *Critical Reviews in Solid State and Materials Sciences* 38, no. 3 (2013): 203-33.
22. Onn, Tzia Ming, Rainer Küngas, Paolo Fornasiero, Kevin Huang, and Raymond J Gorte. "Atomic Layer Deposition on Porous Materials: Problems with Conventional Approaches to Catalyst and Fuel Cell Electrode Preparation." *Inorganics* 6, no. 1 (2018): 34.
23. Fiorentino, Giuseppe, Sten Vollebregt, F. D. Tichelaar, Ryoichi Ishihara, and Pasqualina M. Sarro. "Impact of the Atomic Layer Deposition Precursors Diffusion on Solid-State Carbon Nanotube Based Supercapacitors Performances." *Nanotechnology* 26, no. 6 (2015): 064002.
24. Marichy, Catherine, and Nicola Pinna. "Carbon-Nanostructures Coated/Decorated by Atomic Layer Deposition: Growth and Applications." *Coordination Chemistry Reviews* 257, no. 23 (2013): 3232-53.
25. Guan, Cao, and John Wang. "Recent Development of Advanced Electrode Materials by Atomic Layer Deposition for Electrochemical Energy Storage." *Advanced Science* 3, no. 10 (2016): 1500405.
26. Rasteiro, Letícia F., Md Abdul Motin, Luiz H. Vieira, Elisabete M. Assaf, and Francisco Zaera. "Growth of Zro2 Films on Mesoporous Silica Sieve Via Atomic Layer Deposition." *Thin Solid Films* 768 (2023): 139716.
27. Niinistö, Jaakko, Kaupo Kukli, Maarit Kariniemi, Mikko Ritala, Markku Leskelä, Nicolas Blasco, Audrey Pinchart, Christophe Lachaud, Nadia Laaroussi, Ziyun Wang, and Christian Dussarrat. "Novel Mixed Alkylamido-Cyclopentadienyl Precursors for Ald of Zro2 Thin Films." *Journal of Materials Chemistry* 18, no. 43 (2008): 5243-47.
28. Shim, Joon Hyung, Cheng-Chieh Chao, Hong Huang, and Fritz B. Prinz. "Atomic Layer Deposition of Yttria-Stabilized Zirconia for Solid Oxide Fuel Cells." *Chemistry of Materials* 19, no. 15 (2007): 3850-54.
29. Sempel, Janine D., Marja-Leena Kaariainen, Troy A. Colleran, Alejo M. Lifschitz, and Steven M. George. "Ultrathin Zro2 Thickness Control on Tio2/Zro2 Core/Shell Nanoparticles Using Zro2 Atomic Layer Deposition and Etching." *Journal of Vacuum Science & Technology A* 42, no. 5 (2024).
30. Fan, Mengjie, Yichen Ji, Ajibola Lawal, Omar A. Abdelrahman, Raymond J. Gorte, and John M. Vohs. "Site and Structural Requirements for the Dehydra-Decyclization of Cyclic Ethers on Zro2." *Catalysts* 12, no. 8 (2022): 902.
31. Fan, Mengjie, Ching-Yu Wang, Raymond J. Gorte, and John M. Vohs. "Synthesis of Lewis Acid Sites in Sba-15 and Amorphous Silica Using Vapor Phase Infiltration of Zr and Sn." *Catalysis Letters* 154, no. 6 (2024): 2725-34.
32. Sundqvist, Jonas, Jun Lu, Mikael Ottosson, and Anders Hårsta. "Growth of Sno2 Thin Films by Atomic Layer Deposition and Chemical Vapour Deposition: A Comparative Study." *Thin Solid Films* 514, no. 1 (2006): 63-68.
33. Ramachandran, Ranjith K., Jolien Dendooven, Jonas Botterman, Sreeprasanth Pulinthanathu Sree, Dirk Poelman, Johan A. Martens, Hilde Poelman, and Christophe Detavernier. "Plasma Enhanced Atomic Layer Deposition of Ga2o3 Thin Films." *Journal of Materials Chemistry A* 2, no. 45 (2014): 19232-38.
34. Onn, Tzia Ming, Lisandra Arroyo-Ramirez, Matteo Monai, Tae-Sik Oh, Meghavi Talati, Paolo Fornasiero, Raymond J. Gorte, and Mahmoud M. Khader. "Modification of Pd/Ceo2 Catalyst by Atomic Layer Deposition of Zro2." *Applied Catalysis B: Environmental* 197 (2016): 280-85.
35. Onn, Tzia Ming, Shuyi Zhang, Lisandra Arroyo-Ramirez, Ye Xia, Cong Wang, Xiaoqing Pan, George W. Graham, and Raymond J. Gorte. "High-Surface-Area Ceria Prepared by Ald on Al2o3 Support." *Applied Catalysis B: Environmental* 201 (2017): 430-37.